On the dielectric properties of the spin crossover complex [Fe(bpp)2] [BF4]2

Thomas Guillon, Sébastien Bonhommeau, José Sánchez Costa, Antoine Zwick, Jean-François Létard, Philippe Demont, Gábor Molnár, Azzedine Bousseksou

DOI 10.1002/pssa.200567103

On the dielectric properties of the spin crossover complex $[Fe(bpp)_2]$ $[BF_4]_2$

Thomas Guillon[1], **Sébastien Bonhommeau**[1, 2], **José Sanchez Costa**[3], **Antoine Zwick**[2], **Jean-François Létard**[3], **Philippe Demont**[4], **Gábor Molnár**[1], and **Azzedine Bousseksou**[*, 1]

[1] Laboratoire de Chimie de Coordination, UPR 8241 CNRS, 205 Route de Narbonne, 31077 Toulouse, France
[2] Laboratoire de Physique des Solides de Toulouse, UMR 5477 CNRS, 118 Route de Narbonne, 31062 Toulouse, France
[3] Institut de Chimie de la Matière Condensée de Bordeaux, UPR 9048 CNRS, Université Bordeaux I, 87 Av. du Doc. A. Schweitzer, 33608 Pessac, France
[4] Laboratoire de Physique des Polymères-CIRIMAT, CNRS UMR-5085, 118 Route de Narbonne, 31062 Toulouse, France

PACS 31.15.Ew, 71.15.Mb, 75.30.Wx, 77.22.–d, 78.30.–j

The thermal variation of the dielectric constant in the spin crossover complex $[Fe(bpp)_2]$ $[BF_4]_2$ displays a 16 K large hysteresis loop centered around 178 K corresponding to the spin transition temperatures. Unexpectedly, the dielectric constant has a higher value in the low-spin state. DFT calculations were carried out to determine the microscopic electronic polarizabilities, but these latter could not be correlated with the macroscopic permittivity changes pointing the importance of the effect of the counter-anions which must be necessarily taken into account in future DFT calculations.

1 Introduction

Among bistable molecular materials, spin crossover complexes of $3d^4$–$3d^7$ transition metal ions have been investigated by many research groups [1]. These compounds hold some promise to be used in electronics based memories because the conversion between the high-spin (HS) and the low-spin (LS) states can be detected via a capacitance measurement [2]. This becomes possible because the dielectric constant in the two spin states differs sufficiently. Since optical addressing is a convenient way for information storage, spin crossover complexes undergoing a LIESST (Light Induced Excited Spin State Trapping) effect have received many attention recently [3]. The spin crossover compound $[Fe(bpp)_2]$ $[BF_4]_2$, for which bpp stands for 2,6–bis(pyrazol-3-yl)pyridine, is a particularly interesting example because in this material the light induced metastable HS state decays at relatively high temperatures (ca. 110 K) [4, 5].

In this paper, we report the dielectric properties of the complex $[Fe(bpp)_2]$ $[BF_4]_2$ and correlate the macroscopically measured dielectric permittivity with the microscopic (electronic) polarizability calculated by the single molecule DFT (Density Functional Theory) methodology on the cation $[Fe(bpp)_2]^{2+}$ in the LS and HS states. DFT calculations on this compound have been previously carried out in order to find its free energy [6]. Moreover, DFT methods are also widely used to evaluate and assign the molecular vibrational frequencies [7]. Here, we focus on the determination of electronic polarizabilities.

[*] Corresponding author: e-mail: boussek@lcc-toulouse.fr, Phone: +33 5 61 33 31 53, Fax: +33 5 61 55 30 03

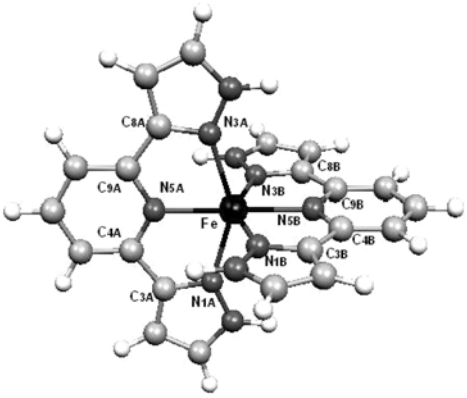

Fig. 1 (online colour at: www.pss-a.com) Optimized structure of the cation $[Fe(bpp)_2]^{2+}$ in the HS state calculated with B3LYP/6-31G*.

2 Experimental section and theoretical methods

The dynamic dielectric spectroscopy method was used to measure the thermal variation of the complex dielectric permittivity ($\varepsilon^* = \varepsilon' - i\varepsilon''$) in the 10^2-10^7 Hz frequency range, successively in the heating and cooling modes by means of a Novocontrol BDS 4000 broadband spectrometer. The frequency sweeps were carried out isothermally. The powder samples were enclosed in a Teflon sample holder between two stainless steel electrodes. Raman spectra were acquired at room temperature and at 80 K using a Dilor XY triplemate micro-spectrograph coupled to a Princeton Instruments CCD detector. The 632.8 nm line of a He–Ne laser was used as the excitation source. DFT calculations have been carried out on single molecules *in vacuo* with Gaussian03 package [8]. The Becke's three-parameter hybrid functional B3LYP [9] was used with the 3–21G and 6–31G* basis sets. The input structures of the cation $[Fe(bpp)_2]^{2+}$ for the optimization of the LS and HS geometries were taken from X-ray crystallographic data (Fig. 1) [10]. The optimized structures were calculated without any constraint. From these structures, polarizabilities and intramolecular vibrational frequencies were determined.

3 Results and discussion

Spin crossover complexes of the family $[Fe(bpp)_2]\,[X]_y \cdot nH_2O$ (where $X = NCS^-$, $NCSe^-$, BF_4^- with $y = 2$ or $X = Fe(CN)_5(NO)^{2-}$ with $y = 1$) were extensively studied by Sugiyarto et al. [10] who reported X-ray crystallographic data for several dehydrated or hydrated compounds ($n = 1$ for NCS^-, $n = 3$ for BF_4^- and $n = 0$ for the other compounds). Unfortunately, single crystal X-ray structures of the title spin crossover compound could not be obtained. However, the crystallographic structure of the cation $[Fe(bpp)_2]^{2+}$ has been determined in several HS or LS compounds with different counter-anions. These X-ray data were used as the input of the DFT calculations and also to check the reliability of the calculated structures of this cation. Tables 1a, b and c provide a comparison between X-ray crystallographic data and calculated bond distances and angles of the cation $[Fe(bpp)_2]^{2+}$. Calculated values of bond distances and angles in the ligand (Table 1b and c) reproduce the measured ones with good accuracy. Calculated values of bond angles involving the central metal atom are in good agreement with the experimental data as well. The metal-ligand bond distances are known to be deeply affected by the spin state change. Indeed, the Fe–N bonds in the HS state are approximately 0.2 Å longer when compared to the LS state both in the experiments and in the calculations (Table 1a). However, the B3LYP/6-31G(d) method slightly overestimates Fe–N bond length values (in both spin states). This tendency was observed earlier for many spin crossover complexes [7]. With this DFT method, the optimized geometry in the LS state presents a D_{2d} symmetry with a good precision. The optimized geometry in the HS state has a slightly lower symmetry (C_{2v}). From these optimized geometries, static electronic polarizability tensors were calculated as the analytic second derivative of the energy with respect to the electric field in order to determine the spin-

Table 1a Experimental Fe–N distances (Å) in some complexes of the $[Fe(bpp)_2][X]_y \cdot nH_2O$ family and calculated values for the $[Fe(bpp)_2]^{2+}$ ion in the HS and LS states. X-ray crystallographic data are given for (1) $[Fe(bpp)_2][NCS]_2 \cdot H_2O$ [10], (2) $[Fe(bpp)_2][NCSe]_2$ [10], (3) $[Fe(bpp)_2][Fe(CN)_5(NO)]$ [10], (4) $[Fe(bpp)_2][BF_4]_2 \cdot 3H_2O$ [10], (5) $[Fe(bpp)_2][Fe(CN)_5(NO)]$ form 1 [10] and (6) $[Fe(bpp)_2][Fe(CN)_5(NO)]$ form 2 [10].

HS state	X-ray[1]	X-ray[2]	X-ray[3]	B3LYP/6-31G*
$Fe-N_{1A}$	2.174 (8)	2.183 (3)	2.189 (3)	2.225
$Fe-N_{3A}$	2.168 (7)	2.198 (3)	2.189 (3)	2.225
$Fe-N_{5A}$	2.112 (8)	2.132 (3)	2.143 (3)	2.143
$Fe-N_{1B}$	2.181 (7)	2.176 (3)	2.189 (3)	2.226
$Fe-N_{3B}$	2.179 (7)	2.182 (3)	2.189 (3)	2.226
$Fe-N_{5B}$	2.126 (7)	2.125 (3)	2.143 (3)	2.141
LS state	**X-ray[4]**	**X-ray[5]**	**X-ray[6]**	**B3LYP/6-31G***
$Fe-N_{1A}$	1.968 (6)	1.976 (2)	1.965 (2)	1.998
$Fe-N_{3A}$	1.968 (6)	1.967 (2)	1.976 (2)	1.998
$Fe-N_{5A}$	1.916 (5)	1.933 (2)	1.933 (2)	1.944
$Fe-N_{1B}$	1.978 (6)	1.976 (2)	1.965 (2)	1.998
$Fe-N_{3B}$	1.974 (6)	1.967 (2)	1.976 (2)	1.998
$Fe-N_{5B}$	1.915 (5)	1.933 (2)	1.933 (2)	1.944

state dependence of the microscopic electrical properties. Furthermore, vibrational frequencies were also calculated and compared to experimental Raman spectra in order to test the validity of the DFT calculations.

Figure 2 presents Raman spectra associated with the pure HS state (200 K), the pure LS state (140 K) and a mixed HS and LS state on the ascending branch of the hysteresis (180 K). Several marker bands can be chosen to follow the spin transition. For example, peaks at 231 cm^{-1} and 1224 cm^{-1} are characteristic of the LS state while the peak at 1577 cm^{-1} only appears in the HS state. However, the most relevant marker bands are located at ca. 670 cm^{-1} and 1030 cm^{-1} and exhibit a well-resolved frequency shift from 667 cm^{-1} to 678 cm^{-1} and from 1019 cm^{-1} to 1034 cm^{-1} when going from the HS to the LS state. An efficient way to assign these modes to atomic motions consists of calculating molecular vibrational frequencies using the DFT methodology. In the calculated spectra two main frequency ranges stand out.

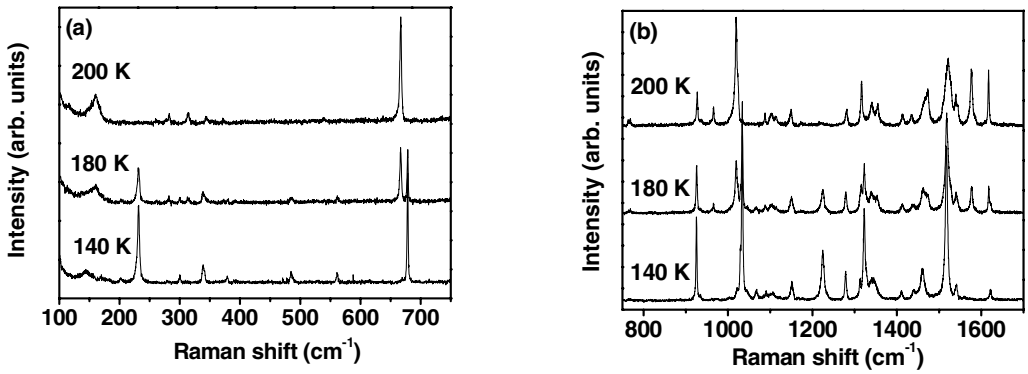

Fig. 2 a) Experimental Raman spectra of $[Fe(bpp)_2][BF_4]_2$ recorded in the 100–750 cm^{-1} frequency range at 140, 180 and 200 K. b) Experimental Raman spectra of the $[Fe(bpp)_2][BF_4]_2$ recorded in the 750–1650 cm^{-1} frequency range at 140, 180 and 200 K.

Table 1b Selected experimental bond distances (Å) and bond angles (degrees) in some HS complexes of the $[Fe(bpp)_2][X]_y \cdot nH_2O$ family and calculated values for the $[Fe(bpp)_2]^{2+}$ ion in the HS state. X-ray crystallographic data are given for (1) $[Fe(bpp)_2][NCS]_2 \cdot H_2O$ [10], (2) $[Fe(bpp)_2][NCSe]_2$ [10], (3) $[Fe(bpp)_2][Fe(CN)_5(NO)]$ [10].

HS state	X-ray(1)	X-ray(2)	X-ray(3)	B3LYP/6-31G*
$N_{1A}-C_{3A}$	1.35 (1)	1.343 (5)		1.350
$C_{3A}-C_{4A}$	1.46 (1)	1.453 (6)		1.468
$N_{5A}-C_{4A}$	1.35 (1)	1.342 (5)		1.349
$N_{5A}-C_{9A}$	1.34 (1)	1.338 (5)		1.349
$C_{8A}-C_{9A}$	1.52 (1)	1.462 (6)		1.468
$N_{3A}-C_{8A}$	1.32 (1)	1.342 (5)		1.350
$N_{1B}-C_{3B}$	1.31 (1)	1.350 (5)		1.350
$C_{3B}-C_{4B}$	1.45 (1)	1.453 (6)		1.468
$N_{5B}-C_{4B}$	1.31 (1)	1.338 (5)		1.349
$N_{5B}-C_{9B}$	1.34 (1)	1.350 (5)		1.349
$C_{8B}-C_{9B}$	1.49 (1)	1.458 (6)		1.468
$N_{3B}-C_{8B}$	1.33 (1)	1.325 (5)		1.350
$N_{1A}-Fe-N_{3A}$	148.2 (3)	147.4 (1)	147.16 (7)	148.3
$N_{1A}-Fe-N_{5A}$	74.1 (3)	73.7 (1)	73.58 (7)	74.1
$N_{1A}-Fe-N_{1B}$	94.9 (3)	94.5 (1)		95.4
$N_{1A}-Fe-N_{5B}$	110.2 (3)	108.6 (1)		105.8
$N_{1B}-Fe-N_{3B}$	147.1 (3)	147.8 (1)	147.16 (7)	148.4
$N_{1B}-Fe-N_{5B}$	73.5 (3)	74.1 (1)	73.58 (7)	74.2
$N_{1B}-Fe-N_{5A}$	108.8 (3)	105.3 (1)		105.9
$N_{3A}-Fe-N_{3B}$	94.5 (3)	94.0 (1)		95.4
$Fe-N_{1A}-C_{3A}$	116.5 (6)	116.3 (3)	116.0 (2)	114.9
$Fe-N_{5A}-C_{4A}$	119.9 (6)	120.0 (3)	119.7 (2)	119.8
$C_{4A}-N_{5A}-C_{9A}$	118.4 (9)	119.9 (3)	120.6 (2)	120.5
$Fe-N_{5A}-C_{9A}$	121.5 (6)	120.1 (3)	119.7 (2)	119.8
$Fe-N_{3A}-C_{8A}$	116.9 (6)	115.7 (2)	116.0 (2)	114.9
$Fe-N_{1B}-C_{3B}$	116.2 (6)	115.8 (3)	116.0 (2)	114.8
$Fe-N_{5B}-C_{4B}$	119.1 (6)	120.0 (3)	119.7 (2)	119.7
$C_{4B}-N_{5B}-C_{9B}$	119.5 (8)	120.1 (4)	120.6 (2)	120.5
$Fe-N_{5B}-C_{9B}$	121.3 (6)	119.9 (3)	119.7 (2)	119.7
$Fe-N_{3B}-C_{8B}$	116.8 (6)	116.2 (3)	116.0 (2)	114.8

The 3220–3670 cm^{-1} frequency range corresponds to C–H and N–H stretches whereas the second range spans up to 1660 cm^{-1}. In this latter frequency range, the major changes in vibrational frequencies occur below 700 cm^{-1} and most of the modes associated with the Fe displacement appear below 500 cm^{-1}. Above 500 cm^{-1}, the calculations gave two vibrational modes exhibiting frequency shifts from 679 cm^{-1} to 689 cm^{-1} and from 1033 cm^{-1} to 1051 cm^{-1} when going from the HS to the LS state. These latter modes can be assigned to nearly symmetric deformations of the pyridine rings coupled to a symmetric stretching of the $N_{5A}-Fe-N_{5B}$ bonds. This coupling revealed by the DFT calculations explains the somewhat surprising large shift of these two modes observed in the experimental spectra.

The thermal bistability of the $[Fe(bpp)_2][BF_4]_2$ spin crossover complex appears clearly through magnetic susceptibility measurements (Fig. 3a). Cooling the sample leads to a sharp decrease in HS fraction around 180 K. The pure LS state is reached at ca. 140 K. From this state, the sample heating yields a rise in the HS fraction around 174 K. The pure HS state is then attained at ca. 194 K. Thermal variations of

Table 1c Selected experimental bond distances (Å) and bond angles (degrees) in some LS complexes of the $[Fe(bpp)_2][X]_y \cdot nH_2O$ family and calculated values for the $[Fe(bpp)_2]^{2+}$ ion in the LS state. X-ray crystallographic data are given for (4) $[Fe(bpp)_2]\,[BF_4]_2 \cdot 3H_2O$ [10], (5) $[Fe(bpp)_2]\,[Fe(CN)_5(NO)]$ form 1 [10] and (6) $[Fe(bpp)_2]\,[Fe(CN)_5(NO)]$ form 2 [10].

LS state	X-ray[4]	X-ray[5]	X-ray[6]	B3LYP/6-31G*
N_{1A}–C_{3A}	1.328 (8)			1.353
C_{3A}–C_{4A}	1.471 (9)			1.462
N_{5A}–C_{4A}	1.352 (8)			1.354
N_{5A}–C_{9A}	1.341 (8)			1.354
C_{8A}–C_{9A}	1.459 (9)			1.462
N_{3A}–C_{8A}	1.342 (8)			1.353
N_{1B}–C_{3B}	1.340 (8)			1.353
C_{3B}–C_{4B}	1.454 (10)			1.462
N_{5B}–C_{4B}	1.369 (9)			1.354
N_{5B}–C_{9B}	1.347 (8)			1.354
C_{8B}–C_{9B}	1.461 (10)			1.462
N_{3B}–C_{8B}	1.347 (8)			1.353
N_{1A}–Fe–N_{3A}	158.2 (2)	157.9 (1)	158.0 (1)	158.4
N_{1A}–Fe–N_{5A}	79.1 (2)	78.9 (1)	78.6 (1)	79.2
N_{1A}–Fe–N_{1B}	92.6 (2)			92.0
N_{1A}–Fe–N_{5B}	101.3 (2)			100.8
N_{1B}–Fe–N_{3B}	158.6 (2)	157.9 (1)	158.0 (1)	158.4
N_{1B}–Fe–N_{5B}	79.3 (2)	79.0 (1)	79.4 (1)	79.2
N_{1B}–Fe–N_{5A}	101.3 (2)			100.8
N_{3A}–Fe–N_{3B}	93.6 (2)			92.0
Fe–N_{1A}–C_{3A}	117.0 (5)	116.8 (1)	115.3 (1)	115.6
Fe–N_{5A}–C_{4A}	119.8 (5)	119.8 (1)	119.8 (1)	119.4
C_{4A}–N_{5A}–C_{9A}	119.6 (6)	120.4 (1)	120.4 (1)	121.1
Fe–N_{5A}–C_{9A}	120.6 (5)	119.8 (1)	119.8 (1)	119.4
Fe–N_{3A}–C_{8A}	115.9 (5)	116.3 (1)	117.6 (1)	115.6
Fe–N_{1B}–C_{3B}	116.3 (5)	116.8 (1)	115.3 (1)	115.6
Fe–N_{5B}–C_{4B}	119.7 (5)	119.8 (1)	119.8 (1)	119.4
C_{4B}–N_{5B}–C_{9B}	120.1 (6)	120.4 (1)	120.4 (1)	121.1
Fe–N_{5B}–C_{9B}	120.1 (5)	119.8 (1)	119.8 (1)	119.4
Fe–N_{3B}–C_{8B}	115.8 (5)	116.3 (1)	117.6 (1)	115.6

the dielectric constant at 100 kHz frequency for $[Fe(bpp)_2]\,[BF_4]_2$ (Fig. 3b) reveal the same transition temperatures (T_{up} = 186 K, T_{down} = 170 K). The dielectric constant in the HS state is smaller than that of the LS state $\Delta\varepsilon' = \varepsilon'_{HS} - \varepsilon'_{LS} = -0.11$. The change in dielectric constant of SCO materials results from structural modifications accompanying the spin state change. Within the investigated frequency range, the dielectric constant and therefore the total polarizability as well are nearly independent of the frequency of the external applied electric field (Fig. 4). No relaxation process, associated with an orientational polarization of permanent dipole moments, is observed either in the absorption curve ε'' vs. the frequency. This absence of spontaneous polarization in the $[Fe(bpp)_2]\,[BF_4]_2$ complex rules out any effect of the dipolar polarization on the observed transition and the polarizability is mainly composed of electronic and ionic contributions thereby. As the HS molecules are more voluminous than the LS ones, their electronic polarizability and hence the relative permittivity should decrease when going from the HS to the LS state. Furthermore, since the HS state has a more ionic nature, the ionic polarizability must also decrease to some extent with the HS $\rightarrow$ LS spin state change. Indeed, for most of the investigated SCO

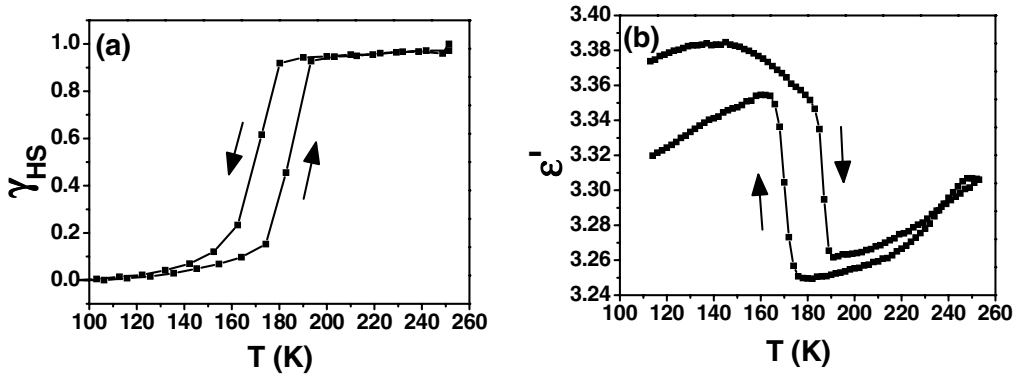

Fig. 3 (online colour at: www.pss-a.com) a) Thermal variation of the proportion of high-spin molecules (γ_{HS}) in $[Fe(bpp)_2]$ $[BF_4]_2$ obtained through magnetic susceptibility measurements. b) Thermal hysteresis of the dielectric constant associated with the spin transition of $[Fe(bpp)_2]$ $[BF_4]_2$.

compounds a decrease of the macroscopically measurable ε' was observed during the HS to LS transition [2]. Therefore the negative value of $\Delta\varepsilon'_{HL}$ observed in the compound $[Fe(bpp)_2]$ $[BF_4]_2$ can be considered as atypical. This behavior was observed earlier only for the spin crossover complex Fe[5-NO_2-sal-N(1, 4, 7, 10)] and assigned to structural modifications through DFT calculations [11]. In fact, the local symmetry distortion modifies significantly the local field, inducing a large change in the dipole moment detected through dielectric spectroscopy. On the contrary, in the case of the $[Fe(bpp)_2]$ $[BF_4]_2$ molecule, we were unable to correlate the microscopic electronic polarizability obtained by DFT calculations with the experimentally observed behavior of the dielectric constant. In fact, the calculated positive value of the mean electronic polarizability change ($\Delta\alpha = \alpha_{HS} - \alpha_{LS} = 7.01$ a.u.) has an opposite sign compared to the variation of the dielectric constant($\Delta\varepsilon' = \varepsilon'_{HS} - \varepsilon'_{LS} = -0.11$).

In summary, this work revealed a clear correlation between the dielectric and magnetic properties of the spin crossover complex $[Fe(bpp)_2]$ $(BF_4)_2$. Interestingly, we have found that the (quasi-static) dielectric constant has a higher value in the LS state. The experimental investigation was completed by DFT calculations on the $[Fe(bpp)_2]^{2+}$ cation. The comparison of these calculations with the experimental results revealed that the molecular geometry and vibrational frequencies of the cation are determined mainly by the spin state and are less influenced by the nature of the actual counter anion. On the other hand, the calculations suggest that lattice effects (such as the position or orientation of the anions, H-bonds, etc.) must have a strong influence on the macroscopic electrical properties. For this reason, alternative methods like introduction of a Madelung field in a molecular DFT calculation [12] or periodic DFT calculations should be used to get a better description of this system. Especially, periodic DFT calculations provide interesting challenge for future research.

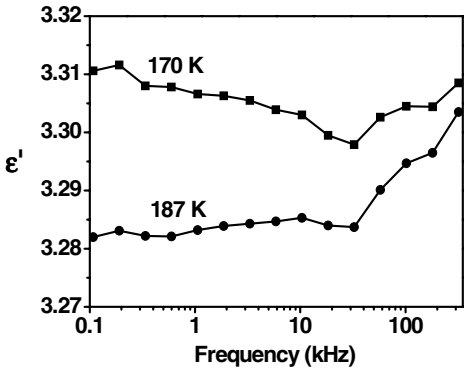

Fig. 4 (online colour at: www.pss-a.com) Frequency dependence of the dielectric constant of the spin crossover compound $[Fe(bpp)_2]$ $[BF_4]_2$ at 186 K (circles) and 170 K (squares).

Acknowledgements DFT calculations have been performed thanks to the facilities provided by CALMIP (Calculs en Midi-Pyrénées, France), CINES (Centre Informatique National de l'Enseignement Supérieur, France) and IDRIS (Institut du Développement et des Ressources en Informatique Scientifique).

References

[1] P. Gütlich and H. A. Goodwin (eds.), Spin Crossover in Transition Metal Compounds I–III, Topics in Current Chemistry, Vol. 233–235 (2004).
[2] A. Bousseksou, G. Molnár, P. Demont, and J. Menegotto, J. Mater. Chem. **13**, 2069 (2003).
[3] A. Hauser, Top. Curr. Chem. **234**, 155 (2004).
[4] S. Marcén, L. Lecren, L. Capes, H. A. Goodwin, and J.-F. Létard, Chem. Phys. Lett. **358**, 87 (2002).
[5] H. A. Goodwin and K. H. Sugiyarto, Chem. Phys. Lett. **139**, 470 (1987).
T. Buchen, P. Gütlich, K. H. Sugiyarto, and H. A. Goodwin, Chem. Eur. J. **2**, 1134 (1996).
T. Buchen, P. Gütlich, and H. A. Goodwin, Inorg. Chem. **33**, 4573 (1994).
[6] H. Paulsen, L. Duelund, H. Winkler, H. Toftlund, and A. X. Trautwein, Inorg. Chem. **40**, 2201 (2001).
[7] G. Baranovic, Chem. Phys. Lett. **369**, 668 (2003).
G. Brehm, M. Reiher, and S. Schneider, J. Phys. Chem. A **106**, 12024 (2002).
V. K. Pálfi, T. Guillon, H. Paulsen, G. Molnár, and A. Bousseksou, C. R. Chimie **8**, 1317 (2005).
H. Paulsen and A. X. Trautwein, Top. Curr. Chem. **235**, 197 (2004).
L. M. Lawson Daku, A. Vargas, A. Hauser, A. Fouqueau, and M. E. Casida, Chem. Phys. **6**, 1393 (2005).
S. Bonhommeau, N. Bréfuel, V. K. Pálfi, G. Molnár, A. Zwick, L. Salmon, J.-P. Tuchagues, J. S. Costa, J.-F. Létard, H. Paulsen, and A. Bousseksou, Phys. Chem. Chem. Phys. **15**, 2909 (2005).
[8] M. J. Frisch et al., GAUSSIAN 03, Revision B.05 (Gaussian, Inc., Pittsburgh, PA, 2003).
[9] A. D. Becke, J. Chem. Phys. **98**, 5648 (1993).
Becke3LYP Method Refs. and General Citation Guidelines, Gaussian News **5**, 2 (1994).
[10] K. H. Sugiyarto, D. C. Craig, A. D. Rae, and H. Goodwin, Aust. J. Chem. **47**, 869 (1994); Aust. J. Chem. **50**, 869 (1997); Aust. J. Chem. **53**, 755 (2000); Dalton Trans. **12**, 2443 (2003).
[11] S. Bonhommeau, T. Guillon, L. M. Lawson Daku, P. Demont, J. Sanchez Costa, J.-F. Létard, G. Molnár, and A. Bousseksou, Angew. Chem. Int. Ed **45**, 1625 (2006); Angew. Chem. **118**, 1655 (2006).
[12] S. Zein, G. S. Matouzenko, and S. A. Borshch, J. Phys. Chem. A **109**, 8568 (2005).